Carbon 221 (2024) 118900

Contents lists available at ScienceDirect

Carbon

journal homepage: www.elsevier.com/locate/carbon

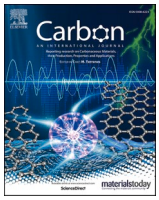

Two-color laser driven enhanced electron emission from carbon nanotubes with long carrier lifetime

Jinxing Cao [a,1], Can Wang [a,1], Feilong Hu [a], Qingbin Zhang [a,*], Peixiang Lu [a,b,c,**]

[a] School of Physics and Wuhan National Laboratory for Optoelectronics, Huazhong University of Science and Technology, Wuhan, 430074, China
[b] Hubei Key Laboratory of Optical Information and Pattern Recognition, Wuhan Institute of Technology, Wuhan, 430205, China
[c] Optics Valley Laboratory, Hubei, 430074, China

ARTICLE INFO

Keywords:
Carbon nanotubes
Ultrafast photoemission
Enhanced photocurrent
Carrier lifetime
Electron sources

ABSTRACT

Ultrafast electron pulses generated using femtosecond lasers offer a direct means for investigating ultrafast processes, but the yield of electron emission remains a significant practical limitation. This study demonstrates a substantial enhancement in yield of electron emission from carbon nanotubes induced by two-color ($\omega + 2\omega$) pulses with an 80 MHz repetition rate and this enhancement is non-delay-dependent. Compared to the sum of photocurrents induced by each color pulse individually, the combined two-color pulses result in a remarkable enhancement in yield of electron emission by more than 25 times. We attribute this enhanced yield to carrier-assisted optical field emission: carbon nanotubes sustain high carrier concentration state under laser radiation thereby enhancing yield of electron emission. We propose the carrier migration emission model to provide a semi-quantitative description for the carrier-assisted optical field emission. This phenomenon introduces a new method to increase the yield of ultrafast electron pulses from CNTs and paves the way for next-generation ultrafast electron emitters and on chip ultrafast optoelectronic device.

1. Introduction

The generation of ultrafast electron pulses (UEPs) induced by ultrashort laser fields on nanoscale tips is a fundamental technique enabling ultrafast imaging and attosecond measurements, such as ultrafast electron microscopy [1–3], PHz electronic devices [4–9], and electromagnetic waveform detectors [10]. The mechanism of ultrafast electron emission induced by ultrashort laser has conventionally been categorized into two regimes: from multiphoton ionization to strong-field tunneling with increasing the strength of incident optical-field [11–20]. In contrast with multiphoton ionization, the photoemission is controlled by the incident optical waveform rather than the envelope of laser pulses in strong-field tunneling regime [21,22]. This characteristic enables the generation of UEPs with optical sub-cycle durations and high optical phase synchronization, thereby achieving attosecond resolution [23]. As a consequence, the stability of electron emitters in strong laser fields becomes crucial for ultrafast electron sources. However, conventional metallic emitters are susceptible to damage caused by laser pulses in the strong-field tunneling regime [24]. In contrast, carbon nanotubes (CNTs) hold promise as ideal emitters in the strong-field tunneling regime due to their high damage threshold [25–27]. Additionally, CNTs possess advantageous properties, including a high aspect ratio [28], wide spectral response [29], and mechanical stability [30], making them suitable candidates for generating more efficient, controllable, and stable UEPs.

Despite CNTs have excellent properties as electron emitters, their electron emission efficiency (average yield of electrons for single laser pulse) remains a significant limitation for the development of ultrafast electron source devices. Enhancing the electron emission efficiency makes it available to use laser with lower pulse energy and helps to mitigate damage from laser fields. In the past, improving the emission efficiency of UEPs has often involved using advanced nanostructures with small tip radii to obtain a higher local field enhancement factor [21,22,31–39]. However, further improvements through this method are

* Corresponding author. School of Physics and Wuhan National Laboratory for Optoelectronics, Huazhong University of Science and Technology, Wuhan 430074, China.
** Corresponding author. School of Physics and Wuhan National Laboratory for Optoelectronics, Huazhong University of Science and Technology, Wuhan 430074, China.
E-mail addresses: zhangqingbin@hust.edu.cn (Q. Zhang), lupeixiang@hust.edu.cn (P. Lu).
[1] These authors contributed equally to this work.

https://doi.org/10.1016/j.carbon.2024.118900
Received 2 September 2023; Received in revised form 2 February 2024; Accepted 2 February 2024
Available online 3 February 2024

challenging due to the extreme tip radius of CNTs is about 1 nm. Modifying the external conditions applied to the emitter can also influence its electron emission efficiency. For instance, the combined laser and static electric fields can be employed to modulate the electron emission yield of CNTs [40,41]. While this method brings limited current enhancement and more complex structures of emitters. Given the longstanding research focus on improving the efficiency of UEPs, further investigation is needed to enhance the emission efficiency of UEPs from CNTs, which are considered superior and promising electron emitters.

In this work, we present a novel approach to substantially improve the emission efficiency of UEPs induced by delayed fundamental (ω) and second harmonic (2ω) femtosecond laser pulses, with a maximum delay of 500 ps. We introduce the concept of carrier-assisted optical field emission as an explanation for the delay-independent enhanced current signal. The emission spot of CNTs sustains a high carrier concentration state under the radiation of 80 MHz laser pulses (with 12.5 ns time-interval between each pulse) due to the nanosecond-scale carrier lifetime of CNTs [42–44]. As a result, a significant enhancement of emission efficiency occurs even with large delay for two-color pulses. In this experiment, 30 times or even higher enhancement of current was obtained, compared to sum of current induced by individual pulse. The electron emission current from CNTs can reach 20th order of laser field strength. Furthermore, we investigate electron emission efficiency from CNTs using various repetition rate combinations of incident two-color pulses. As expected, this phenomenon does not occur when using non-temporal overlap 1 kHz two-color pulses because of their long pulse time-interval (~1 ms). We propose carrier migration emission (CME) model to provide a semi-quantitative description of this carrier-assisted optical field emission. This research demonstrates that pulse time-interval significantly impacts the electron emission efficiency in systems with long carrier lifetimes. For a given carrier lifetime, sufficiently short pulse time-interval can markedly improve the electron emission efficiency. These findings are crucial for enhancing the overall performance of ultrafast electronic sources and advancing the development of PHz operating frequency devices.

2. Experimental section

Diagram of electron emission from CNT is depicted in Fig. 1(a). The two-color pulses, 800 nm (ω) and 400 nm (2ω), are used to induce electron emission from the CNTs. The samples (purchased from Kenye Technology), single-walled carbon nanotube arrays are grown vertically on highly doped n-type silicon wafers with an area of 0.5 cm × 0.5 cm and a thickness of 0.5 mm. The height of the CNT clusters is about 100 μm, as shown in Fig. 1(b). The diameter of the nanotubes (d) ranged from 0.78 to 2.53 nm according to the radial breathing mode frequency ($\omega_{RBM} = 248/d(cm^{-1}nm^{-1})$) in Raman spectra is evaluated (see Fig. S1) [45]. The measured work function of CNTs is 4.42 eV (see Fig. S2). Fig. 1 (c) is the scheme of experimental setup. Our experiments were carried out in a low-vacuum chamber (0.1 Torr) and at room temperature. The cathode (CNT sample) was fixed on insulated specimen holder which is made of PEEK (Polyether ether ketone). To precisely adjust the location of the focal spot on the sample, the specimen holder was fixed on a three-dimensional nano-positioning stage capable of movements with a

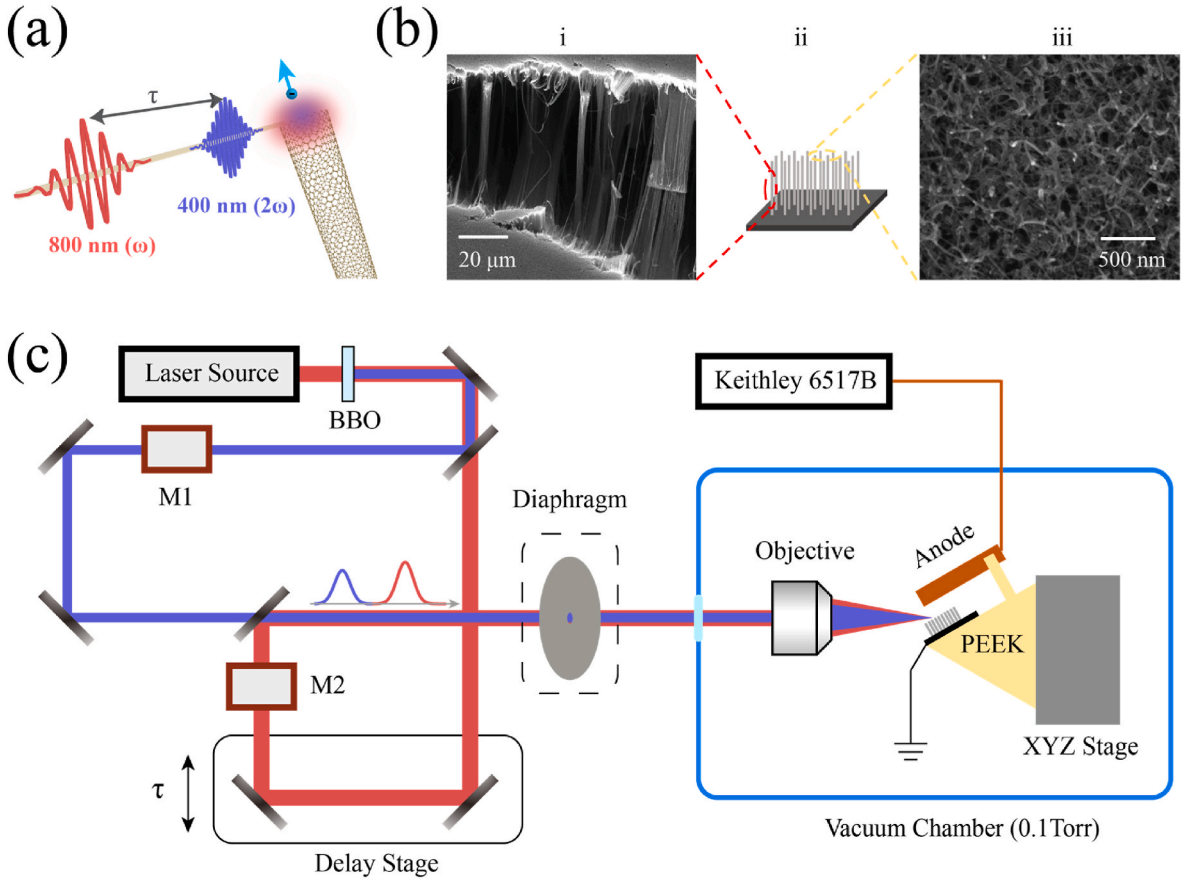

Fig. 1. Using two-color laser pulses to generate photocurrent from CNTs. (a) Diagram of electron emission from CNT. The same polarized $\omega + 2\omega$ two color laser field, with a delay τ, was focused on the CNT resulting in electron emission from the CNT-tip. (b) Scheme and SEM images of the sample. i. Longitudinal sections image of the vertically CNT-arrays, scale bar 20 μm; ii. Diagram of the vertically CNT-arrays grown on Si wafer; iii. SEM image at the top of the CNTs, scale bar 500 nm. (c) Scheme of experimental setup when using 80 MHz laser pulse. The diaphragm, outlined with a dotted line, replaces the objective specifically when using 1 kHz laser pulses.

minimum step size of 30 nm. The anode was a permalloy plate with an area of 1 cm × 3 cm and a thickness of 1 mm, and it was positioned 2 mm away from the CNT arrays to collect emitted electrons.

The laser pulse trains with different repetition rates were employed to change average pulse time-interval in our experiment. The high repetition rate laser is delivered by a laser oscillator with a repetition rate of 80 MHz, while the low repetition rate laser is delivered by a Ti: sapphire amplifier with a repetition rate of 1 kHz. The temporal delay between both laser fields is controlled by a Mach-Zehnder interferometer. The objective (ThorLabs LMM40X–UVV) and diaphragm were used to illuminate laser pulse on the sample through 2 mm gap between cathode and anode. The choice between using the objective or diaphragm was dependent on whether we were utilizing 80 MHz or 1 kHz laser pulses, respectively. The objective with a focal length of 5 mm was positioned inside the vacuum chamber and the location of diaphragm was positioned outside vacuum chamber as shown in Fig. 1(c). In our measurements, the diameters of focal spot were achieved to be 4 μm for the ω laser pulse and 2 μm for the 2ω laser pulse respectively. Due to such small focal spot and high nonlinearity of the current, we estimate that the number of CNTs contributing electron emission in the focal spot is less 10 when using 80 MHz laser. The diaphragm reduced the laser beam diameter to 1 mm, allowing the laser beam to pass through 2 mm gap between cathode and anode. The number of CNTs contributing to electron emission illuminated by 1 kHz laser was $\sim 10^5$ times that illuminated by 80 MHz laser. The durations of the ω and 2ω pulses are approximately 100 fs (see Fig. S3). These two pulses are highly spatially overlapped, and their intensities and polarizations can be individually adjusted. This adjustment is achieved using M1 and M2, each comprising a polarizer and two half-wave plates. The 2ω field has a fixed phase relation with respect to ω field due to parametric process for generating second harmonic [46]. Therefore, the ω and 2ω fields remain phase synchronization even if the carrier envelope phase (CEP) is not stable.

In the strong-field tunneling regime, electrons are emitted from CNTs only when the electric field points into the CNTs (downward-bent potential). The emitted electrons move toward the anode and generate current signal. We employed source measurement unit (Keithley 6517B) to apply bias voltage and measure the current signals on the anode. A 5 V bias voltage was applied to facilitate the electron collection. The noise signal was ~0.5 pA measured in the vacuum chamber with laser turned off. In our experiment the gas discharge can be excluded because the peak field of laser pulse (less than 0.5 V/nm) was far below the threshold of gas discharge (more than 10 V/nm) and no gas discharge signal was observed.

3. Results and discussion

When irradiating the CNTs with a 1 kHz two-color laser, a noticeable delay-dependent photocurrent is observed, as illustrated in Fig. 2(a). The two-color laser field comprises pulses at frequencies ω and 2 ω. The optical delay between the two fields is well controlled by a linear translation stage, with resolution of 0.66 fs. We observe an enhancement of the current signals in regions where ω and 2ω pulses are temporally overlapped, and this enhancement depends on the delay between the two fields. Similar to experiments conducted with metal emitters [47],

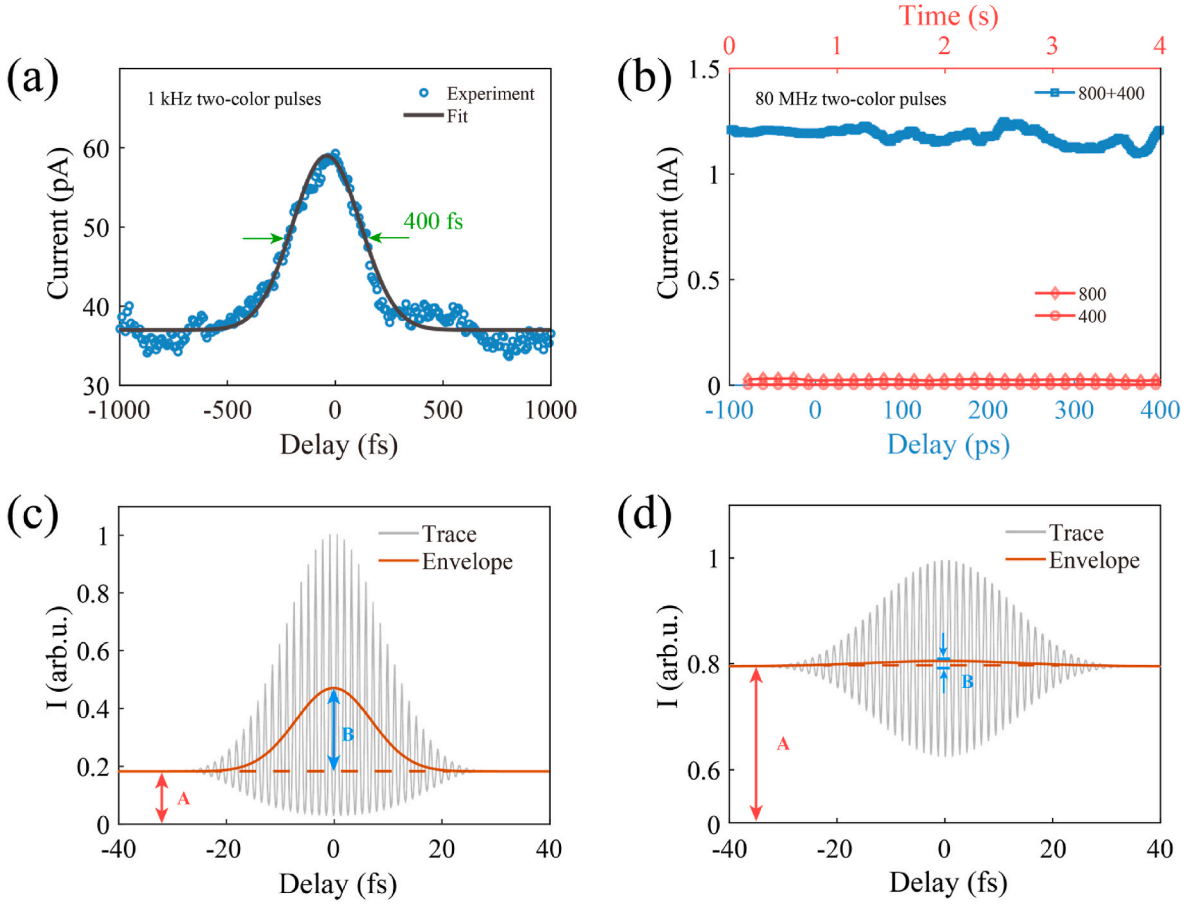

Fig. 2. Current signals as a function of delay. (a) Blue circles are measured current signals induced by 1 kHz ω and 2ω pulses. Black curve is the gaussian fit of the current signal. FWHM is about 400 fs. (b) Blue curve is the current signals induced 80 MHz ω and 2ω pulses. Red rhombus and circle markers are the photocurrent excited by separate pulses as a function of time. (c), (d) The results of calculation for FN (Fowler-Nordheim) model and CME model respectively. Gray solid lines are the calculated current signals and orange solid lines correspond to the experimental measurements.

we fit the delay-dependent current signals using a Gaussian function:

$$G = A + B\exp\left(-(\tau-\tau_0)^2/D^2\right) \quad (1)$$

with A the offset, B the peak height, τ_0 the delay offset, and D the width. Besides, we define the enhancement factor of current signals as $M = I_{\omega+2\omega}/(I_\omega + I_{2\omega})$ to quantify the enhancement of emission efficiency. $I_{\omega+2\omega}$ represents total current induced by the two laser pulses and $I_\omega + I_{2\omega}$ represents sum of current induced by individual pulses. In Fig. 2(a), the DC offset $I_\omega + I_{2\omega}$ is represented by A, the amplitude of the current signal variation $(I_{\omega+2\omega})_{max} - (I_\omega + I_{2\omega})$ is represented by B and D corresponds to the width of the enhanced current. The full width at half maximum (FWHM) of the enhanced current signal is about 400 fs, approximately 200 fs longer than the pulse duration, which agrees with the dephasing time of the CNTs [48]. The ratio of A to B corresponds to the enhancement factor M. In this experiment, similar delay-dependent current signals are observed using different intensity combinations of the two-color pulses. The range of laser intensity covers both the multi-photon regime and the strong-field tunneling regime. More details are provided in Fig. S3.

However, when using the combination of 80 MHz two-color pulses delivered by the oscillator, the current signals exhibit distinct features compared to those shown in Fig. 2(a). These features are as follows: (i) The two-color field increases the emission rate by more than ten times, even when the two fields have a considerable delay that thousand times than pulse duration. (ii) It becomes hard to distinguish delay-dependent current signals from the measurement noise because the variation in current signals within the temporal overlap of the two-color pulses is too small. As shown in Fig. 2(b), $I_{\omega+2\omega}$ remains around 1.2 nA, and the current enhancement factor M stays approximately 30 within the delay range of zero to several hundreds of picoseconds. The currents I_ω and $I_{2\omega}$ induced by the separated pulses are 10 pA and 30 pA, respectively. The regime of photoemission is marked by the Keldysh parameters $\gamma = \omega\sqrt{2m\Phi}/e\beta F$ (ω is optical frequency, Φ is work function, m is the mass of electron and e is its charge, β is the field enhancement factor). In this case, the power of ω and 2ω laser pulses are 3 mW and 0.5 mW, respectively, resulting in $\gamma_\omega = 0.8$ and $\gamma_{2\omega} = 2$, supporting strong field tunneling. This non-delay-dependent enhanced current signals may represent an intriguing process of ultrafast electron emission.

Traditionally, for femtosecond pulses, the impact arising from varying repetition rates of the incident laser (ranging from kHz to MHz) was commonly disregarded. An underlying factor is that the pulse time-interval was generally much larger than the carrier lifetime of the emitters. The carrier lifetime induced by incident lasers in metallic nanostructures is usually less than 1 ps [49]. However, for CNTs, some experiments have shown that the carrier lifetime can be on the nano-second scale or even up to 100 ns [42]. Given that the pulse time-interval of 12.5 ns of the 80 MHz laser pulse is comparable to the carrier's lifetime in CNTs, we hypothesize that this unique phenomenon is mainly caused by the cooperative interaction of pulse time-interval and carrier lifetime. Additionally, the combination of the two pulses facilitates the study of this process. Based on this assumption, we propose CME model to semi-quantitatively calculate the ultrafast electron emission in the system of 80 MHz laser-excited CNTs (theory section for details). While for CNTs excited by a 1 kHz laser, the traditional FN (Fowler-Nordheim) model is applicable [50]. Fig. 2(c) and (d) show the results of calculation for the FN model and CME model, respectively. In this simulation, the pulse durations are decreased to $\tau_\omega = 52$ fs and $\tau_{2\omega} = 26$ fs to ensure good visibility. Both pulses are still within the multi-cycle regime, and this does not affect the feature of calculated results. The gray solid lines represent the current trace as a function of delay, while the orange solid lines represent the envelope signal of the current (G in equation (1)). The photocurrent measured in the experiment corresponds to the orange solid line, and the oscillations in the optical sub-cycle are absent due to the complex energy band structure of CNTs. The envelope line in Fig. 2(c) provides a good agreement with the delay-dependent current signal in (a). As shown in Fig. 2(d), B/A is significantly reduced compared to that in (c), consistent with the faint delay-dependence of current signals in (b). CME model provides a description for the disappearing delay-dependence of electron emission using 80 MHz two-color laser pulses and the huge enhancement of current signals will be specified in Fig. 5.

The experiments investigating CNTs excited by different repetition rate combinations of two-color pulses were conducted to study the influence of the cooperative interaction of pulse time-interval and carrier's lifetime on the efficiency of electron emission, as illustrated in Fig. 3. Fig. 3(a) and (b) show the current signals excited by the non-temporally overlapped (temporally overlapped) combination of 1 kHz ω and 2ω pulses in the same experiment, respectively. The horizontal coordinate represents the time of measurement. When the two pulses are non-temporally overlapped, no enhancement is observed, i.e. $M \approx 1$. Similar to Fig. 2(a), as the delay approaches zero (center of temporal overlap), M increases to 1.2, demonstrating that the enhancement is delay-dependent. The current signals induced by 80 MHz 2ω pulses and 1 kHz ω pulses with non-temporal overlap are shown in Fig. 3(c), with $M \approx 3.7$. This enhancement is larger than that of the combination of the two-color 1 kHz pulses shown in Fig. 3(a) and (b) and it is non-delay-dependent. Considering the average pulse time-interval, combining the 80 MHz and 1 kHz pulses induces little change in the average pulse time-interval compared to the 80 MHz pulse alone. Under our assumption, the carrier's concentration excited by these two pulses is almost equal to that excited by the 80 MHz pulse individually. Consequently, the electron emission yield induced by the 80 MHz 2ω pulses remains almost unchanged, while that induced by the 1 kHz ω pulses is greatly enhanced. Only considering the enhancement factor of I_ω, $(I_{\omega+2\omega} - I_{2\omega})/I_\omega \approx 22$. Fig. 3(d) displays the current signals induced by the combination of 80 MHz two-color pulses, with $M \approx 25$. These experimental results demonstrate that the repetition rate of incident pulses plays a crucial role in the enhancement of current signals. We consider that the emission point of CNTs has high carrier concentration excited by the pulses with a repetition rate of 80 MHz, significantly promoting electron emission efficiency.

To describing the cooperative interaction of pulse time-interval and carrier's lifetime on electron emission, we employ carrier migration emission model (CME model) to semi-quantitatively calculate the electron emission efficiency. Fig. 4illustrates the schematic diagram of optical field emission under low repetition and high repetition rate pulse, respectively. In Fig. 4(a), the orange line represents the allowed bands for CNTs, while the blue shaded area represents electron-filling states of the valence band (VB), and the pink area corresponds to electron-filling states of the conduction band (CB). For low repetition rate pulses, the CB electron population remains unaffected and is almost in thermodynamic equilibrium. Electron tunneling occurs due to the relatively low barrier height induced by the laser field. However, for high repetition rate pulses, the CB electron population persists at relatively high levels excited by the frequent pulses and this promotes electron tunneling, as shown in Fig. 4(b). The decay formula describing the variation in the electron population is defined as follows:

$$Z(E,t) = \exp\left(-(t-t_0)/\tau\right)Z(E,t_0) \quad (2)$$

with τ the lifetime of carriers, $Z(E,t_0)$ the variation in electron distribution caused by the pulse at time t_0. When the second pulse is applied at time t, the pulse time-interval $T = t - t_0$. For low repetition rate pulse, $T \gg \tau$, the carriers excited by the previous pulse have almost vanished by the time the next pulse is applied. For high repetition rate pulse, $T \approx \tau$, part of the carriers excited by the previous pulse are still residual when the next pulse is applied. After a sufficient number of pulses, the carriers will reach a relatively stable high concentration state.

CME model regards the state of electrons as a functional of $f_0(E)$, which could be used to describe the transition of carrier (electron or hole) in energy band for solid under strong fields. The initial state of the

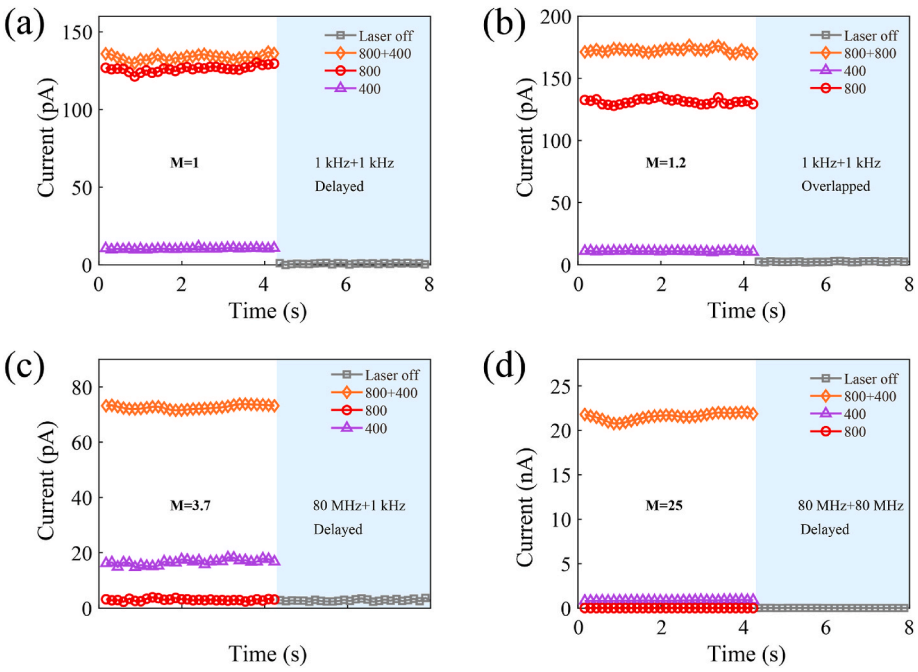

Fig. 3. Current signals induced by different repetition rate combinations of two-color pulses. (a), (b) Measured current signals using temporally overlapped or delayed 1 kHz ω and 2ω pulses respectively. Rhombus markers are the current induced by the combine of two-color pulses. Triangle and circle markers are the current induced by separated pulses, M is 1 or 1.2, respectively. (c) Current induced by delayed 80 MHz 2ω pulses and 1 kHz ω pulses, M is 3.7. (d) Current induced by delayed 80 MHz ω and 2ω pulses, M is 25.

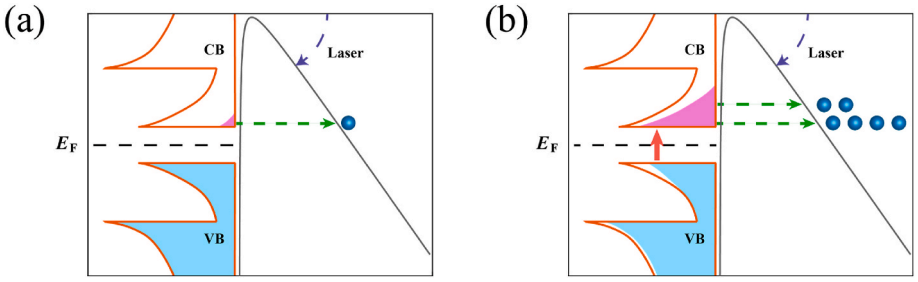

Fig. 4. Schematic diagram of CNT optical field emission. (a) Diagram of electron emission excited by laser pulse with a relatively low repetition rate. Orange line represents allowed bands and shaded areas (CB-pink and VB-blue) represent electron-filling states. Gray line is the potential barrier effected by laser field. Blue balls represent the tunneling electrons. (b) Diagram of electron emission excited by laser pulse with a relatively high repetition rate. Electrons population in CB is higher than that in (a). (A colour version of this figure can be viewed online.)

electron population in CME model is given by the following equation:

$$f_0(E) = D(E)F(E,T) \tag{3}$$

with $D(E)$ the DOS of SWCNT, $F(E,T)$ the Fermi-Dirac distribution at temperature T. When the energy of an electron is greater than the work function of solid, the electron is considered to be excited to the continuous state and emitted into vacuum.

This model has the following assumptions: (i) Under the action of an external field, the proportion of electrons excited on a certain energy level, or the probability P of electron absorption of photons, is proportional to the laser intensity; (ii) Electrons can only be excited to energy levels with holes; (iii) The energy difference between the initial state and the higher state which the electron is excited depends on the energy of the photon, and the energy distribution of photons depends on the spectral intensity.

According to the above assumptions, if the electron population distribution is $f_n(\varepsilon)$ and the hole distribution is $k_n(\varepsilon) = 1 - f_n(\varepsilon)$ when the number of experienced pulses is n, the electron population for $n+1$ pulses:

$$f_{n+1}(E) = \int [(1-P)f_n(\varepsilon)\delta(E-\varepsilon) + Pf_n(\varepsilon)\sigma(E-\varepsilon_0)k_n(\varepsilon)]d\varepsilon \tag{4}$$

For right side of equation (4) the first term represents unexcited electrons, while the second term represents excited electrons, which the proportion of excited electrons is P. The spectral distribution is $\sigma(\varepsilon)$, and the photon energy is ε_0. $\sigma(E-\varepsilon_0)$ represents the probability that an electron with energy E will gain one photon energy. When the action of the last pulse was completed, we obtained $Z(E,t_0) = f_{n+1}(E) - f_n(E)$ and bring this to equation (2) for next step of calculation.

In CME model we consider one ω pulse and one 2ω pulse as a set of pulses. Every set of pulses is applied on CNTs, carriers are generated. In order to determine the electron emission efficiency of the nth set of pulses, we calculate the carrier distribution that has been excited by the previous n-1 sets of pulses. The electron emission based on the carrier concentration is calculated using the FN model.

$$I_{FN}(\mathrm{E}) \propto F(t)^2 \Theta(-F(t)) \exp\left(\left(4\sqrt{2m(\Phi-E)^3}\right) \Big/ 3\hbar e F(t)\right) \tag{5}$$

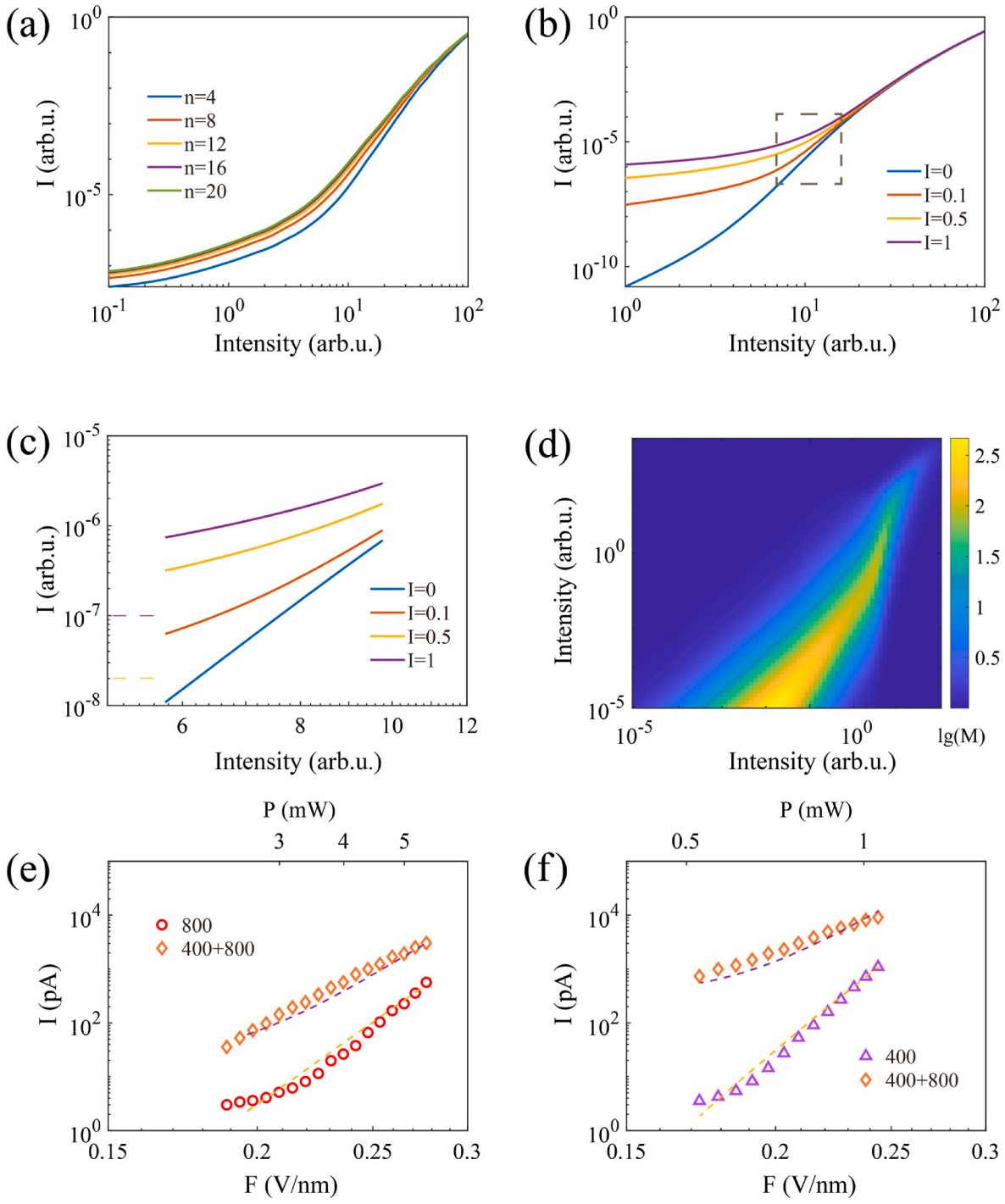

Fig. 5. Simulation results of CME model and compared with experiments. (a) Cumulative effect of laser pulse on electron emission efficiency. (b) Laser-intensity-dependence of electron emission efficiency calculated by CME model. Horizontal coordinate is the intensity of ω pulses. Legend represents different intensities of second harmonic pulse. (c) Results of calculation inside the dashed line in (b). The purple dashed line and the yellow dashed line are the electron emission efficiency induced by the 2ω pulses individually (without ω pulses). (d) The enhancement of electron emission efficiency at different ratios of $\omega + 2\omega$ pulses calculated by CME model. (e), (f) Comparison of experimental data and results of calculation.

$$I_{CME} = \int I_{FN}(E) \bullet f_{n-1}(E) dE \tag{6}$$

with $\Theta(-F(t))$ the Heaviside step function, m the mass of electron, $F(t)$ the local enhanced field, Φ the work function of the CNTs and E the energy level of the carriers (taking the Fermi energy as 0). The electron emission efficiency for each set of pulses can be obtained from equation (6).

The results of calculation based on CME model are presented in Fig. 5. Fig. 5(a) illustrates the calculated efficiency of electron emission for the nth pulse set using CME model. As the number of pulse sets increases, the efficiency of electron emission tends to saturate. In the experiments using 80 MHz laser pulses, we assume that the lifetime of carriers for CNTs is 10 ns, and the emission efficiency becomes saturated after tens of pulse sets. Fig. 5(b) displays the electron emission efficiency for different fixed 2ω pulse intensities when varying the ω pulse

intensity using CME model. The horizontal axis represents the relative intensity of the field. As the ω pulse intensity increases, the total electron emission efficiency also increases, but the enhancement factor M decreases. When the ω pulse intensity becomes sufficiently high, the total electron emission efficiency becomes almost identical to that induced by ω pulses individually. Moreover, we calculated the enhancement factor M under a wider range of two-color pulse intensity ratios, as depicted in Fig. 5(d). As the intensities of each pulse increase, the enhancement factor M decreases. To achieve ideal enhancement factors, the intensities of the two pulses need to match the proper ratio.

Due to the potential damage to CNTs caused by excessively high laser intensity and the limitations of the measurement device's resolution, we validated our theoretical calculations within a relatively narrow range of laser intensities in the experiments. Fig. 5(c) corresponds to the red dashed line in Fig. 5(b) and can be considered as the range of light intensities measured in the experiment. By fixing the intensity of 2ω pulses and varying the intensity of ω pulses, we obtained the current signal dependent with field strength, as shown in Fig. 5(e). The power of 2ω pulses was fixed at 0.2 mW, corresponding to a Keldysh parameter of $\gamma \approx 3$. While the power of ω pulses ranged from 2.5 mW to 5.5 mW, Keldysh parameters γ ranging from 0.5 to 0.8. The dashed line represents the result of the CME model calculation in Fig. 5(e). With the increasing intensity of ω pulse, the predictions of CME model closely aligned with the experimental data, particularly in aspects of nonlinearity and the current enhancement factor. Similarly, Fig. 5(f) shows the result obtained by fixing the intensity of ω pulses and varying the intensity of 2ω pulses. The power of ω pulses was fixed at 2.7 mW, and the power of 2ω pulses ranged from 0.5 mW to 1 mW. The CME model is suitable for semi-quantitative analysis of the enhanced photoemission observed in our experiment, thus supporting the carrier-assisted optical field emission.

4. Conclusion

In conclusion, our investigation focused on the effect of carrier lifetime and pulse repetition rate on the efficiency of laser-induced ultrafast electron pulses (UEPs) generation from carbon nanotubes (CNTs). A remarkable enhancement in the emission efficiency of UEPs was observed when using delayed two-color pulses with a high repetition rate (80 MHz), resulting in an enhancement factor of current signals (M) ranging from 10 to 100. However, this significant enhancement disappeared when using 1 kHz two-color pulses. The pulse repetition rate played a crucial role in this enhancement, and the pulse time-interval becoming close to the carrier's lifetime led to increased carrier concentration in the emitters, which promoted the enhanced photoemission. To describe the enhancement of photoemission considering the effect of carrier's lifetime, we propose the carrier migration emission (CME) model. The simulation results of CME model were found to be in good agreement with the experimental results. We demonstrate a meaningful approach to increase the generation rate of UEPs through using emitters with long carrier lifetime and incident pulses with high repetition rate. Our experiments and theoretical model indicate that carriers play a significant role in ultrafast electron emission. Additionally, it provides new design possibilities for electronic source devices and on-chip ultrafast detectors.

CRediT authorship contribution statement

Jinxing Cao: Writing – review & editing, Writing – original draft, Visualization, Validation, Methodology, Investigation, Formal analysis, Data curation, Conceptualization. **Can Wang:** Writing – review & editing, Visualization, Validation, Methodology, Investigation, Formal analysis, Data curation, Conceptualization. **Feilong Hu:** Validation, Supervision, Methodology, Data curation, Conceptualization. **Qingbin Zhang:** Writing – review & editing, Validation, Supervision, Resources, Project administration, Methodology, Investigation, Funding acquisition, Formal analysis, Conceptualization. **Peixiang Lu:** Supervision, Resources, Project administration, Funding acquisition.

Declaration of competing interest

The authors declare that they have no known competing financial interests or personal relationships that could have appeared to influence the work reported in this paper.

Acknowledgments

This work was supported by the National Key Research and Development Program of China (Grant No. 2023YFA1406800) and the National Natural Science Foundation of China (NSFC) (Grant No. 92150106, No. 11934006, No. 12021004, No. 11627809) and the Innovation Project of Optics Valley Laboratory (Grant No. OVL2021ZD001).

Appendix A. Supplementary data

Supplementary data to this article can be found online at https://doi.org/10.1016/j.carbon.2024.118900.

References

[1] A.H. Zewail, Four-dimensional electron microscopy, Science 328 (2010) 187–193.
[2] G.M. Vanacore, A.W.P. Fitzpatrick, A.H. Zewail, Four-dimensional electron microscopy: ultrafast imaging, diffraction and spectroscopy in materials science and biology, Nano Today 11 (2016) 228–249.
[3] M.T. Hassan, J.S. Baskin, B. Liao, A.H. Zewail, High-temporal-resolution electron microscopy for imaging ultrafast electron dynamics, Nat. Photonics 11 (2017), 425-+.
[4] C. Karnetzky, P. Zimmermann, C. Trummer, C.D. Sierra, M. Worle, R. Kienberger, A. Holleitner, Towards femtosecond on-chip electronics based on plasmonic hot electron nano-emitters, Nat. Commun. 9 (2018) 7.
[5] T. Rybka, M. Ludwig, M.F. Schmalz, V. Knittel, D. Brida, A. Leitenstorfer, Sub-cycle optical phase control of nanotunnelling in the single-electron regime, Nat. Photonics 10 (2016) 667–670.
[6] T. Higuchi, C. Heide, K. Ullmann, H.B. Weber, P. Hommelhoff, Light-field-driven currents in graphene, Nature 550 (2017), 224-+.
[7] F. Krausz, M.I. Stockman, Attosecond metrology: from electron capture to future signal processing, Nat. Photonics 8 (2014) 205–213.
[8] M. Ludwig, G. Aguirregabiria, F. Ritzkowsky, T. Rybka, D.C. Marinica, J. Aizpurua, A.G. Borisov, A. Leitenstorfer, D. Brida, Sub-femtosecond electron transport in a nanoscale gap, Nat. Phys. 16 (2020), 341-+.
[9] D.C. Mor, Y.J. Yang, F. Ritzkowsky, F.X. Kartner, K.K. Berggren, N.K. Singh, P. D. Keathley, PHz electronic device design and simulation for waveguide-integrated carrier-envelope phase detection, J. Lightwave Technol. 40 (2022) 3823–3831.
[10] M.R. Bionta, F. Ritzkowsky, M. Turchetti, Y.J. Yang, D.C. Mor, W.P. Putnam, F. X. Kartner, K.K. Berggren, P.D. Keathley, On-chip sampling of optical fields with attosecond resolution, Nat. Photonics 15 (2021) 787.
[11] Corkum, Plasma perspective on strong field multiphoton ionization, Phys. Rev. Lett. 71 (1993) 1994–1997.
[12] Schafer, Yang, DiMauro, Kulander, Above threshold ionization beyond the high harmonic cutoff, Phys. Rev. Lett. 70 (1993) 1599–1602.
[13] Corkum, Burnett, Brunel, Above-threshold ionization in the long-wavelength limit, Phys. Rev. Lett. 62 (1989) 1259–1262.
[14] Walker, Sheehy, DiMauro, Agostini, Schafer, Kulander, Precision measurement of strong field double ionization of helium, Phys. Rev. Lett. 73 (1994) 1227–1230.
[15] C.I. Blaga, F. Catoire, P. Colosimo, G.G. Paulus, H.G. Muller, P. Agostini, L. F. DiMauro, Strong-field photoionization revisited, Nat. Phys. 5 (2009) 335–338.
[16] L.V. Keldysh, Ionization in the field of a strong electromagnetic wave, Zh. Eksperim. i Teor. Fiz. 47 (1964).
[17] M.F. Ciappina, J.A. Perez-Hernandez, A.S. Landsman, W.A. Okell, S. Zherebtsov, B. Foerg, J. Schoetz, L. Seiffert, T. Fennel, T. Shaaran, T. Zimmermann, A. Chacon, R. Guichard, A. Zair, J.W.G. Tisch, J.P. Marangos, T. Witting, A. Braun, S.A. Maier, L. Roso, M. Kruger, P. Hommelhoff, M.F. Kling, F. Krausz, M. Lewenstein, Attosecond physics at the nanoscale, Rep. Prog. Phys. 80 (2017) 50.
[18] M. Krüger, C. Lemell, G. Wachter, J. Burgdörfer, P. Hommelhoff, Attosecond physics phenomena at nanometric tips 51 (2018) 172001.
[19] M.F. Ciappina, J.A. Pérez-Hernández, A.S. Landsman, W.A. Okell, S. Zherebtsov, B. Foerg, J. Schoetz, L. Seiffert, T. Fennel, T. Shaaran, T. Zimmermann, A. Chacón, R. Guichard, A. Zaïr, J.W.G. Tisch, J.P. Marangos, T. Witting, A. Braun, S.A. Maier, L. Roso, M. Krüger, P. Hommelhoff, M.F. Kling, F. Krausz, M. Lewenstein, Attosecond physics at the nanoscale, Rep. Prog. Phys. 80 (2017).
[20] W.P. Putnam, R.G. Hobbs, P.D. Keathley, K.K. Berggren, F.X. Kärtner, Optical-field-controlled photoemission from plasmonic nanoparticles, Nat. Phys. 13 (2017) 335–339.

[21] G. Herink, D.R. Solli, M. Gulde, C. Ropers, Field-driven photoemission from nanostructures quenches the quiver motion, Nature 483 (2012) 190–193.
[22] M. Kruger, M. Schenk, P. Hommelhoff, Attosecond control of electrons emitted from a nanoscale metal tip, Nature 475 (2011) 78–81.
[23] H.Y. Kim, M. Garg, S. Mandal, L. Seiffert, T. Fennel, E. Goulielmakis, Attosecond field emission, Nature 613 (2023) 662–666.
[24] M. Sivis, M. Duwe, B. Abel, C. Ropers, Extreme-ultraviolet light generation in plasmonic nanostructures, Nat. Phys. 9 (2013) 304–309.
[25] S. Hong, S. Myung, Nanotube electronics - a flexible approach to mobility, Nat. Nanotechnol. 2 (2007) 207–208.
[26] A.V. Eletskii, Carbon nanotube-based electron field emitters, Phys. Usp. 53 (2010) 863–892.
[27] W. Zhu, C. Bower, O. Zhou, G. Kochanski, S. Jin, Large current density from carbon nanotube field emitters, Appl. Phys. Lett. 75 (1999) 873–875.
[28] R.F. Zhang, Y.Y. Zhang, Q. Zhang, H.H. Xie, W.Z. Qian, F. Wei, Growth of half-meter long carbon nanotubes based on Schulz-Flory distribution, ACS Nano 7 (2013) 6156–6161.
[29] C. Li, X. Zhou, F. Zhai, Z.J. Li, F.R. Yao, R.X. Qiao, K. Chen, M.T. Cole, D.P. Yu, Z. P. Sun, K.H. Liu, Q. Dai, Carbon nanotubes as an ultrafast emitter with a narrow energy spread at optical frequency, Adv. Mater. 29 (2017) 6.
[30] R.H. Baughman, A.A. Zakhidov, W.A. de Heer, Carbon nanotubes - the route toward applications, Science 297 (2002) 787–792.
[31] R. Bormann, M. Gulde, A. Weismann, S.V. Yalunin, C. Ropers, Tip-enhanced strong-field photoemission, Phys. Rev. Lett. 105 (2010) 4.
[32] M. Schenk, M. Kruger, P. Hommelhoff, Strong-field above-threshold photoemission from sharp metal tips, Phys. Rev. Lett. 105 (2010).
[33] S.V. Yalunin, M. Gulde, C. Ropers, Strong-field photoemission from surfaces: theoretical approaches, Phys. Rev. B 84 (2011) 14.
[34] M. Kruger, M. Schenk, M. Forster, P. Hommelhoff, Attosecond physics in photoemission from a metal nanotip, J. Phys. B Atom. Mol. Opt. Phys. 45 (2012) 15.
[35] F. Schertz, M. Schmelzeisen, M. Kreiter, H.J. Elmers, G. Schonhense, Field emission of electrons generated by the near field of strongly coupled plasmons, Phys. Rev. Lett. 108 (2012) 5.
[36] D.J. Park, B. Piglosiewicz, S. Schmidt, H. Kollmann, M. Mascheck, C. Lienau, Strong field acceleration and steering of ultrafast electron pulses from a sharp metallic nanotip, Phys. Rev. Lett. 109 (2012) 5.
[37] P. Dombi, A. Horl, P. Racz, I. Marton, A. Trugler, J.R. Krenn, U. Hohenester, IEEE in ultrafast strong-field photoemission from plasmonic nanoparticles, in: 10th Conference on Lasers and Electro-Optics Pacific Rim (CLEO-PR), Kyoto, JAPAN, Jun 30-Jul 04; IEEE, Kyoto, JAPAN, 2013.
[38] P.M. Nagel, J.S. Robinson, B.D. Harteneck, T. Pfeifer, M.J. Abel, J.S. Prell, D. M. Neumark, R.A. Kaindl, S.R. Leone, Surface plasmon assisted electron acceleration in photoemission from gold nanopillars, Chem. Phys. 414 (2013) 106–111.
[39] B. Piglosiewicz, S. Schmidt, D.J. Park, J. Vogelsang, P. Gross, C. Manzoni, P. Farinello, G. Cerullo, C. Lienau, Carrier-envelope phase effects on the strong-field photoemission of electrons from metallic nanostructures, Nat. Photonics 8 (2014) 38–43.
[40] B.H. Son, D.J. Park, Y.H. Ahn, Electronic control of ultrafast field emission in carbon nanotube gaps, Appl. Phys. Lett. 115 (2019) 5.
[41] D.A. Lyashenko, Y.P. Svirko, M.I. Petrov, A.N. Obraztsov, The laser assisted field electron emission from carbon nanostructure, Journal of the European Optical Society-Rapid Publications 13 (2017).
[42] D.J. Bindl, A.J. Ferguson, M.Y. Wu, N. Kopidakis, J.L. Blackburn, M.S. Arnold, Free carrier generation and recombination in polymer-wrapped semiconducting carbon nanotube films and heterojunctions, J. Phys. Chem. Lett. 4 (2013) 3550–3559.
[43] I. Sarpkaya, Z.Y. Zhang, W. Walden-Newman, X.S. Wang, J. Hone, C.W. Wong, S. Strauf, Prolonged spontaneous emission and dephasing of localized excitons in air-bridged carbon nanotubes, Nat. Commun. 4 (2013).
[44] S. Reich, M. Dworzak, A. Hoffmann, C. Thomsen, M.S. Strano, Excited-state carrier lifetime in single-walled carbon nanotubes, Phys. Rev. B 71 (2005).
[45] K.H. Liu, W.L. Wang, M.H. Wu, F.J. Xiao, X.P. Hong, S. Aloni, X.D. Bai, E.G. Wang, F. Wang, Intrinsic radial breathing oscillation in suspended single-walled carbon nanotubes, Phys. Rev. B 83 (2011) 4.
[46] A. Baltuska, T. Fuji, T. Kobayashi, Controlling the carrier-envelope phase of ultrashort light pulses with optical parametric amplifiers, Phys. Rev. Lett. 88 (2002).
[47] P. Dienstbier, T. Paschen, P. Hommelhoff, Two-color coherent control in photoemission from gold needle tips, J. Phys. B Atom. Mol. Opt. Phys. 54 (2021) 7.
[48] M.W. Graham, Y.Z. Ma, A.A. Green, M.C. Hersam, G.R. Fleming, Pure optical dephasing dynamics in semiconducting single-walled carbon nanotubes, J. Chem. Phys. 134 (2011) 13.
[49] M.L. Brongersma, N.J. Halas, P. Nordlander, Plasmon-induced hot carrier science and technology, Nat. Nanotechnol. 10 (2015) 25–34.
[50] R.H. Fowler, L. Nordheim, Containing papers of a mathematical; character, Electron emission in intense electric fields 119 (1928) 173–181.